

Microscopic spin-wave theory for yttrium-iron garnet films

A. Kreisel^a, F. Sauli, L. Bartosch, and P. Kopietz

Institut für Theoretische Physik, Universität Frankfurt, Max-von-Laue Strasse 1, 60438 Frankfurt, Germany

Received 22 May 2009

Published online 11 August 2009 – © EDP Sciences, Società Italiana di Fisica, Springer-Verlag 2009

Abstract. Motivated by recent experiments on thin films of the ferromagnetic insulator yttrium-iron garnet (YIG), we have developed an efficient microscopic approach to calculate the spin-wave spectra of these systems. We model the experimentally relevant magnon band of YIG using an effective quantum Heisenberg model on a cubic lattice with ferromagnetic nearest neighbour exchange and long-range dipole-dipole interactions. After a bosonization of the spin degrees of freedom via a Holstein-Primakoff transformation and a truncation at quadratic order in the bosons, we obtain the spin-wave spectra for experimentally relevant parameters without further approximation by numerical diagonalization, using efficient Ewald summation techniques to carry out the dipolar sums. We compare our numerical results with two different analytic approximations and with predictions based on the phenomenological Landau-Lifshitz equation.

PACS. 75.10.Jm Quantized spin models – 75.30.Ds Spin waves – 05.30.Jp Boson systems

1 Introduction

In a recent series of experiments [1–5] Demokritov and co-workers discovered strong correlations of highly occupied magnon states in thin films of the magnetic insulator yttrium-iron garnet (YIG) with stoichiometric formula $Y_3Fe_2(FeO_4)_3$. They suggested an interpretation of their results in terms of Bose-Einstein condensation of magnons at room temperature. For a proper interpretation of these experiments, a peculiar feature of the energy dispersion $E_{\mathbf{k}}$ of the relevant magnon band in finite YIG films is important: due to a subtle interplay between finite-size effects, short-range exchange interactions, and long-range dipole-dipole interactions, $E_{\mathbf{k}}$ exhibits a local minimum at a finite wave-vector \mathbf{k}_{\min} , for a certain range of orientations of the external magnetic field \mathbf{H}_e relative to the sample. The existence of such a dispersion minimum has been predicted by Kalinikos and Slavin [6,7] within a phenomenological approach based on the Landau-Lifshitz equation. Unfortunately, such a phenomenological approach does not provide a microscopic understanding of correlation effects, which might be important to explain some aspects of experiments probing the non-equilibrium behaviour of the magnon gas in YIG [1–5,8–11]. This has motivated us to study this problem within the framework of the usual $1/S$ -expansion for ordered quantum spin systems, which is based on the bosonization of an effective microscopic Heisenberg model using either the Holstein-Primakoff [12] or the Dyson-Maleev transformation [13,14], and the subsequent classification of the interaction processes in powers of the small parameter $1/S$.

The $1/S$ -expansion has been extremely successful to understand spin-wave interactions in ordered magnets [15,16]. Previously, several authors have used this approach to calculate spin-wave spectra in ultrathin ferromagnetic films with exchange and dipole-dipole interactions [17–20]. Moreover, interaction effects such as energy shifts and damping of spin-waves in thin films have also been calculated within the $1/S$ -expansion [21,22]. However, in order to apply this approach to realistic models for experimentally relevant YIG films with a thickness of a few microns (corresponding to a few thousand lattice spacings), one has to evaluate numerically rather large dipolar sums [23] to set up the secular matrix whose eigenvalues determine the magnon modes, see equation (18) below. We use here an efficient Ewald summation technique [24] to carry out these summations, which enables us to calculate the spin-wave dispersions of realistic YIG films. Given our numerical results, we can assess the validity of various analytical approximations such as the uniform mode approximation [6,20,25] and the lowest eigenmode approximation.

The rest of this paper is organized as follows: in Section 2 we introduce the effective Heisenberg model which we shall use to describe the experimentally relevant magnon band in YIG. We set up the $1/S$ -expansion and derive the secular equation which determines the magnon dispersion. In Section 3 we present our results for the magnon spectra of YIG. We first discuss our numerical results, which are obtained by evaluating the roots of the secular determinant without further approximation, using the Ewald summation technique described in the appendix to evaluate the necessary dipolar sums. We then discuss in Sections 3.2 and 3.3 two approximate analytical methods for obtaining the dispersion of the lowest magnon band.

^a e-mail: kreisel@itp.uni-frankfurt.de

A comparison with our numerical results allows us to estimate the accuracy of these approximations. Finally, in Section 4 we present our conclusions and give an outlook for further research.

2 Effective Hamiltonian for YIG films

Experimental and theoretical research on YIG has a long history, as reviewed, for example, in reference [26]. Some distinct advantages of YIG are that this material can be grown in very pure crystals and has a very narrow ferromagnetic resonance line, indicating very low spin-wave damping. Actually, YIG is a ferrimagnet at accessible magnetic fields and has a rather complicated crystal structure with space group $Ia3d$ (see Refs. [26,27]) and 20 magnetic ions in the primitive cell. Fortunately, on the energy scales relevant to experiments [1–5,8–11] only the lowest magnon band is important, so that we can describe the physical properties of YIG at room temperature in terms of an effective spin S quantum Heisenberg ferromagnet on a cubic lattice with lattice spacing [27]

$$a = 12.376 \text{ \AA}. \quad (1)$$

The effective Hamiltonian contains both exchange and dipole-dipole interactions,

$$\begin{aligned} \hat{H} = & -\frac{1}{2} \sum_{ij} J_{ij} \mathbf{S}_i \cdot \mathbf{S}_j - \mu \mathbf{H}_e \cdot \sum_i \mathbf{S}_i \\ & - \frac{1}{2} \sum_{ij, i \neq j} \frac{\mu^2}{|\mathbf{R}_{ij}|^3} \left[3(\mathbf{S}_i \cdot \hat{\mathbf{R}}_{ij})(\mathbf{S}_j \cdot \hat{\mathbf{R}}_{ij}) - \mathbf{S}_i \cdot \mathbf{S}_j \right], \end{aligned} \quad (2)$$

where the sums are over the sites \mathbf{R}_i of the lattice and $\hat{\mathbf{R}}_{ij} = \mathbf{R}_{ij}/|\mathbf{R}_{ij}|$ are unit vectors in the direction of $\mathbf{R}_{ij} = \mathbf{R}_i - \mathbf{R}_j = x_{ij}\mathbf{e}_x + y_{ij}\mathbf{e}_y + z_{ij}\mathbf{e}_z$. Here, $\mu = g\mu_B$ is the magnetic moment associated with the spins, where g is the effective g -factor and $\mu_B = e\hbar/(2mc)$ is the Bohr magneton. The exchange energies $J_{ij} = J(\mathbf{R}_i - \mathbf{R}_j)$ decay rapidly with distance, so that it is sufficient to include only nearest neighbour exchange couplings in equation (2), setting $J_{ij} = J$ if \mathbf{R}_i and \mathbf{R}_j are nearest neighbours, and $J_{ij} = 0$ otherwise. Note that we neglect surface anisotropies which might be present in experiments, especially at the surface of the film which is attached to the substrate. Experimentally, the material YIG is characterized by its saturation magnetization [28]

$$4\pi M_S = 1750 \text{ G}, \quad (3)$$

and the exchange stiffness ρ_{ex} of long-wavelength spin-waves [29],

$$\frac{\rho_{\text{ex}}}{\mu} = \frac{J S a^2}{\mu} \approx 5.17 \times 10^{-13} \text{ Oe m}^2. \quad (4)$$

If we arbitrarily set the effective g -factor equal to two [28] so that $\mu = 2\mu_B$, we obtain from equations (3) and (4) for

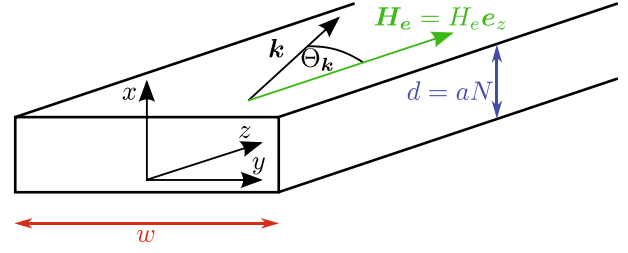


Fig. 1. (Color online) Orientation of our coordinate system for an infinitely long stripe of width w and thickness d . We assume that the external magnetic field $H_e \mathbf{e}_z$ is parallel to the long axis (which we call the z -axis) of the stripe.

the effective spin

$$S = \frac{M_S a^3}{\mu} \approx 14.2, \quad (5)$$

and for the nearest neighbour exchange coupling

$$J = 1.29 \text{ K}. \quad (6)$$

Our above estimates for S and J differ slightly from the values given in reference [30]. Note that the effective spin $S \approx 14.2$ is quite large, so that an expansion in powers of $1/S$ is justified. Introducing the dipolar tensor $D_{ij}^{\alpha\beta} = D^{\alpha\beta}(\mathbf{R}_i - \mathbf{R}_j)$,

$$\begin{aligned} D_{ij}^{\alpha\beta} &= (1 - \delta_{ij}) \frac{\mu^2}{|\mathbf{R}_{ij}|^3} \left[3\hat{R}_{ij}^\alpha \hat{R}_{ij}^\beta - \delta^{\alpha\beta} \right] \\ &= (1 - \delta_{ij}) \mu^2 \frac{\partial^2}{\partial R_{ij}^\alpha \partial R_{ij}^\beta} \frac{1}{|\mathbf{R}_{ij}|}, \end{aligned} \quad (7)$$

we can write our effective Hamiltonian (2) in the compact form

$$\hat{H} = -\frac{1}{2} \sum_{ij} \sum_{\alpha\beta} \left[J_{ij} \delta^{\alpha\beta} + D_{ij}^{\alpha\beta} \right] S_i^\alpha S_j^\beta - h \sum_i S_i^z, \quad (8)$$

where the z -axis of our coordinate system points into the direction defined by the magnetic field \mathbf{H}_e and we have introduced the associated Zeeman energy,

$$h = \mu |\mathbf{H}_e|. \quad (9)$$

We have thus related the set of parameters a, S, J, h appearing in our effective Hamiltonian to experimentally measurable quantities.

To proceed, we restrict ourselves to the description of an infinitely long stripe of width w and thickness $d = Na$, consisting of N layers. For the stripe geometry shown in Figure 1 where the magnetic field points in any direction parallel to the stripe the classical ground-state is a saturated ferromagnet. Therefore we can expand the Hamiltonian in terms of bosonic operators describing fluctuations around the classical groundstate, using either the Holstein-Primakoff or Dyson-Maleev transformation [15,16]. The resulting bosonized spin Hamiltonian is of the form

$$\hat{H} = H_0 + \sum_{n=2}^{\infty} \hat{H}_n. \quad (10)$$

It turns out that Holstein-Primakoff and Dyson-Maleev transformations give different results for \hat{H}_n with $n \geq 4$, but the expressions for \hat{H}_2 and \hat{H}_3 are identical in both transformations. The classical ground state energy is

$$H_0 = -\frac{S^2}{2} \sum_{ij} \left[J_{ij} + D_{ij}^{zz} + \frac{2J_{ij} - D_{ij}^{zz}}{2S} \right], \quad (11)$$

and the quadratic part of the Hamiltonian reads

$$\hat{H}_2 = \sum_{ij} \left[A_{ij} b_i^\dagger b_j + \frac{B_{ij}}{2} (b_i b_j + b_i^\dagger b_j^\dagger) \right], \quad (12)$$

with

$$A_{ij} = \delta_{ij} h + S \left(\delta_{ij} \sum_n J_{in} - J_{ij} \right) + S \left[\delta_{ij} \sum_n D_{in}^{zz} - \frac{D_{ij}^{xx} + D_{ij}^{yy}}{2} \right], \quad (13a)$$

$$B_{ij} = -\frac{S}{2} [D_{ij}^{xx} - 2iD_{ij}^{xy} - D_{ij}^{yy}]. \quad (13b)$$

Since $\hat{H}_n/S^2 = \mathcal{O}(1/S^{n/2})$ and the effective S is large, we expect accurate results even if we only keep the first two terms. In order to proceed we have to keep in mind that a stripe with thickness d and width w is obviously not translationally invariant, so that we cannot simply use a full Fourier transform to diagonalize the Hamiltonian. Because in the experimentally studied samples [1–5,8–11] the width w of the stripe is much larger than the thickness d , we can assume that w is practically infinite, so that our system can be considered to have discrete translational invariance in the y - and z -directions. We may then partially diagonalize \hat{H}_2 in equation (12) by performing a partial Fourier transformation in the yz -plane. Setting $\mathbf{R}_i = (x_i, \mathbf{r}_i)$ with $\mathbf{r}_i = (y_i, z_i)$, and introducing the two-dimensional wave-vector $\mathbf{k} = (k_y, k_z)$ in the yz -plane, we expand

$$b_i = \frac{1}{\sqrt{N_y N_z}} \sum_{\mathbf{k}} e^{i\mathbf{k} \cdot \mathbf{r}_i} b_{\mathbf{k}}(x_i), \quad (14)$$

where N_y and N_z is the number of lattice sites in y and z direction. Our Hamiltonian \hat{H}_2 in equation (12) takes then the form

$$\begin{aligned} \hat{H}_2 = & \sum_{\mathbf{k}} \sum_{x_i, x_j} \left[A_{\mathbf{k}}(x_{ij}) b_{\mathbf{k}}^\dagger(x_i) b_{\mathbf{k}}(x_j) \right. \\ & + \frac{B_{\mathbf{k}}(x_{ij})}{2} b_{\mathbf{k}}(x_i) b_{-\mathbf{k}}(x_j) \\ & \left. + \frac{B_{\mathbf{k}}^*(x_{ij})}{2} b_{\mathbf{k}}^\dagger(x_i) b_{-\mathbf{k}}^\dagger(x_j) \right], \quad (15) \end{aligned}$$

with the amplitude factors [21,22]

$$\begin{aligned} A_{\mathbf{k}}(x_{ij}) = & \sum_{\mathbf{r}} e^{-i\mathbf{k} \cdot \mathbf{r}} A(x_i - x_j, \mathbf{r}), \\ = & S J_{\mathbf{k}}(x_{ij}) + \delta_{ij} [h + S \sum_n D_0^{zz}(x_{in})] \\ & - \frac{S}{2} [D_{\mathbf{k}}^{xx}(x_{ij}) + D_{\mathbf{k}}^{yy}(x_{ij})], \quad (16a) \end{aligned}$$

$$\begin{aligned} B_{\mathbf{k}}(x_{ij}) = & \sum_{\mathbf{r}} e^{-i\mathbf{k} \cdot \mathbf{r}} B(x_i - x_j, \mathbf{r}) \\ = & -\frac{S}{2} [D_{\mathbf{k}}^{xx}(x_{ij}) - 2iD_{\mathbf{k}}^{xy}(x_{ij}) - D_{\mathbf{k}}^{yy}(x_{ij})], \quad (16b) \end{aligned}$$

and the exchange matrix

$$\begin{aligned} J_{\mathbf{k}}(x_{ij}) = & J [\delta_{ij} \{6 - \delta_{j1} - \delta_{jN} \\ & - 2(\cos(k_y a) + \cos(k_z a))\} - \delta_{ij+1} - \delta_{ij-1}]. \quad (17) \end{aligned}$$

3 Spin-wave spectra of YIG

3.1 Numerical approach

If the lattice has N sites in the x -direction, then for fixed two-dimensional wave-vector \mathbf{k} there are N allowed magnon energies $E_{n\mathbf{k}}$, $n = 0, \dots, N-1$, which are given by the positive zeros of the secular determinant

$$\det \begin{pmatrix} E_{\mathbf{k}} - \mathbf{A}_{\mathbf{k}} & -\mathbf{B}_{\mathbf{k}} \\ -\mathbf{B}_{\mathbf{k}}^* & -E_{\mathbf{k}} - \mathbf{A}_{\mathbf{k}} \end{pmatrix} = 0. \quad (18)$$

Here, the $N \times N$ -matrices $\mathbf{A}_{\mathbf{k}}$ and $\mathbf{B}_{\mathbf{k}}$ are defined by

$$[\mathbf{A}_{\mathbf{k}}]_{ij} = A_{\mathbf{k}}(x_{ij}), \quad (19a)$$

$$[\mathbf{B}_{\mathbf{k}}]_{ij} = B_{\mathbf{k}}(x_{ij}), \quad (19b)$$

where $1 \leq i, j \leq N$ label now the lattice sites in the x -direction. The condition (18) follows simply from the fact that the magnon energies can be identified with the poles of the propagators of the Gaussian field theory defined by the quadratic Hamiltonian (15). Note that for $N=1$ the condition (18) correctly reduces to the diagonalization of the Hamiltonian (15) via Bogoliubov transformation. To obtain the complete magnon spectrum of the thin film ferromagnet we have to calculate the dipolar matrices in equation (16b) which leads to the calculation of the following dipolar sums for fixed x_{ij} ,

$$\begin{aligned} D_{\mathbf{k}}^{\alpha\beta}(x_{ij}) = & \sum'_{\mathbf{r}_{ij}} e^{-i\mathbf{k} \cdot \mathbf{r}_{ij}} D_{ij}^{\alpha\beta} \\ = & -\mu^2 \sum'_{y_{ij}, z_{ij}} e^{-i(k_y y_{ij} + k_z z_{ij})} \\ & \times \left[\frac{\delta^{\alpha\beta}}{(x_{ij}^2 + y_{ij}^2 + z_{ij}^2)^{3/2}} - \frac{3r_{ij}^\alpha r_{ij}^\beta}{(x_{ij}^2 + y_{ij}^2 + z_{ij}^2)^{5/2}} \right], \quad (20) \end{aligned}$$

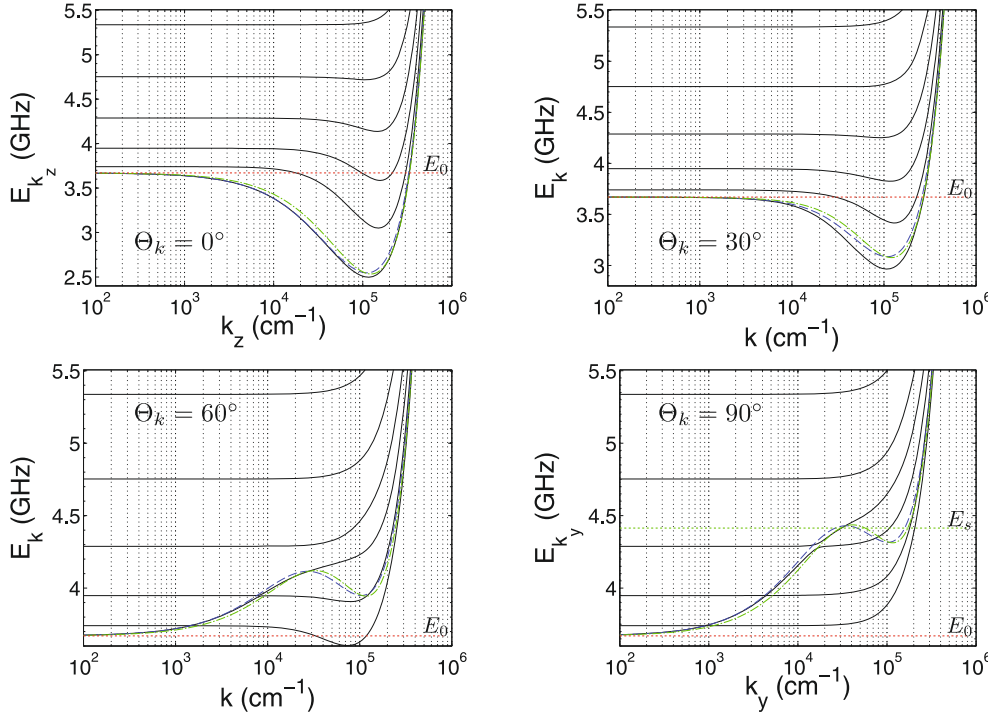


Fig. 2. (Color online) Spin-wave dispersion of a YIG film with thickness $d = 400a \approx 0.495 \mu\text{m}$ in a magnetic field of 700 Oe for wave-vectors in the plane of the film and for different propagation angles $\Theta_{\mathbf{k}} = 0^\circ, 30^\circ, 60^\circ, 90^\circ$ relative to the magnetic field (from top left to bottom right). The black solid curves represent the results from the numerical approach for the lowest modes. The other curves are obtained from equation (36) using the approximation equation (31) (dashed) and equation (47) (dash dotted) for the form factor $f_{\mathbf{k}}$. The thick dotted line labelled E_0 marks the energy of the ferromagnetic resonance given by equation (21); the thick dotted line labelled E_s is the energy $E_s = h + \Delta/2$ of the classical surface mode for $\Theta_{\mathbf{k}} = 90^\circ$ at large wave-vectors, see equations (22, 23).

where \sum' excludes the term $y_{ij} = z_{ij} = 0$ when $x_{ij} = 0$. As these sums are slowly converging and previously used summation techniques [22] are not very efficient for small wave-vectors needed for the dipolar-dominated spectrum of YIG, we use the Ewald summation technique to obtain fast convergence. Details of the calculation can be found in the appendix. To determine the dispersion of all modes we numerically calculate the roots of equation (18) which can be easily done up to a film thickness $d \approx 7 \mu\text{m}$. Using the fact that $\mu/h \approx 2.803 \times 10^{-3} \text{ GHz/Oe}$ we plot all results in units of GHz which is most convenient for experiments using microwave resonators and antennas to detect magnetic excitations. Typical magnon dispersions for different angles $\Theta_{\mathbf{k}}$ between the propagation direction and the magnetic field are shown in Figure 2 for a film with thickness $d = 400a$. Since our approach includes all effects of the exchange and the dipolar interaction within linear spin wave theory, it reproduces semiclassical approximations based on the Landau-Lifshitz equation at long wave-lengths. In particular, for $\mathbf{k} \rightarrow 0$ the dispersion of the lowest mode approaches, independently of the thickness d , the classical ferromagnetic resonance energy

$$E_0 = \sqrt{h(h + \Delta)}, \quad (21)$$

where we introduced the characteristic magnon energy due to dipolar interactions,

$$\Delta = 4\pi\mu M_S. \quad (22)$$

The energy E_0 is indicated as a dotted line in Figure 2. The spacing between different magnon modes decreases with increasing film thickness d ; for example in Figure 3 we show the magnon spectrum of a film with thick-

ness $d = 4040a = 5 \mu\text{m}$, which forms already a quasi-continuum for energies close to the ferromagnetic resonance. Moreover in the regime $dk \ll 1$ one observes that the energy of the n th mode deviates from the first mode by an energy $\Delta E_n = \rho_{\text{ex}}\pi^2 n^2/d^2$ which reflects the well known quadratic behaviour of ferromagnetic spin waves in three dimensions.

Of particular interest is the lowest magnon mode, whose dispersion is illustrated in Figure 4. For propagation directions parallel to the magnetic field ($\Theta_{\mathbf{k}} = 0$) we recover the well known [6] minimum of the lowest magnon mode at a finite wave-vector \mathbf{k}_{min} where large magnon densities have been detected by their microwave radiance [1,5]. As illustrated in Figure 5, the position of the minimum depends on the film thickness as expected and is less pronounced for ultrathin films. With increasing propagation angle $\Theta_{\mathbf{k}}$ the minimum becomes more shallow and completely disappears for $\Theta_{\mathbf{k}} = 90^\circ$. From Figures 2 and 3 it is also obvious that for angles $\Theta_{\mathbf{k}} > 45^\circ$ the lowest modes shift upwards and tend to hybridize with higher modes. However, in the absence of additional symmetries the energy levels never cross. The magnon modes with finite group velocities $\mathbf{v}_g(\mathbf{k}) = \nabla_{\mathbf{k}} E_{\mathbf{k}}$ tend upwards and form the quasi-continuous surface mode. There are no further hybridizations as soon as the mode energies reach the energy

$$E_s = h + \Delta/2 \quad (23)$$

of the classical surface mode.

3.2 Uniform mode approximation

The dispersion of the lowest magnon band can be derived from an effective in-plane Hamiltonian using various

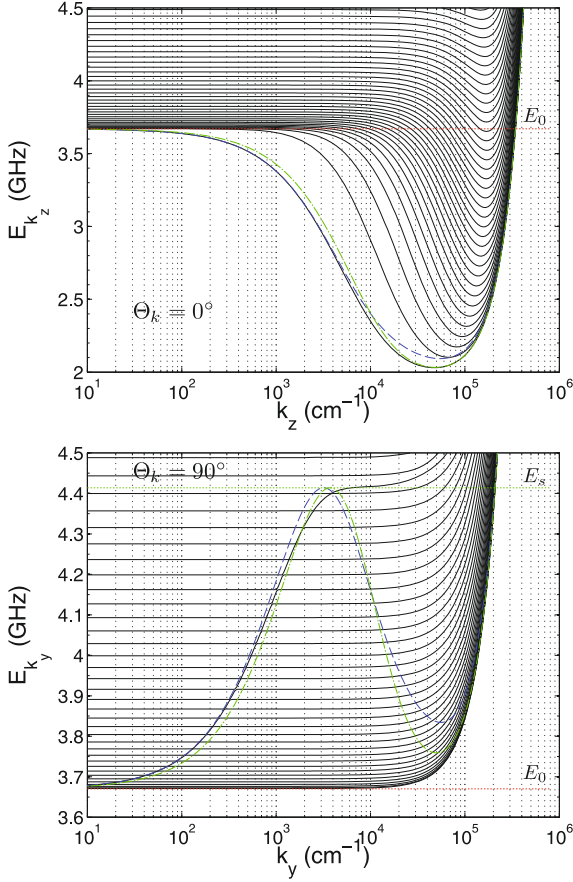


Fig. 3. (Color online) Spin-wave dispersion of a YIG film with thickness $d = 4040a = 5 \mu\text{m}$ for wave-vectors parallel to the external field $H_e = 700 \text{ Oe}$ for $\Theta_k = 0^\circ$ (top) and for $\Theta_k = 90^\circ$ (bottom).

approximations. In fact, at long wavelengths the dispersion of the lowest magnon band can also be obtained within the macroscopic approach based on the Landau-Lifshitz equation [6]. In the simplest approximation, we ignore the fact that the system is not translationally invariant in the x -direction and approximate the corresponding eigenfunctions by plane waves. The lowest magnon band is then obtained by replacing the operators $b_{\mathbf{k}}(x_i)$ in equation (15) by

$$b_{\mathbf{k}}(x_i) \approx \frac{1}{N} \sum_j b_{\mathbf{k}}(x_j) \equiv \frac{1}{\sqrt{N}} b_{\mathbf{k}}. \quad (24)$$

Then equation (15) reduces to

$$\hat{H}_2^{\text{eff}} = \sum_{\mathbf{k}} \left[A_{\mathbf{k}} b_{\mathbf{k}}^\dagger b_{\mathbf{k}} + \frac{B_{\mathbf{k}}}{2} b_{\mathbf{k}} b_{-\mathbf{k}} + \frac{B_{\mathbf{k}}^*}{2} b_{\mathbf{k}}^\dagger b_{-\mathbf{k}}^\dagger \right], \quad (25)$$

with

$$A_{\mathbf{k}} = \frac{1}{N} \sum_{ij} A_{\mathbf{k}}(x_{ij}), \quad (26a)$$

$$B_{\mathbf{k}} = \frac{1}{N} \sum_{ij} B_{\mathbf{k}}(x_{ij}). \quad (26b)$$

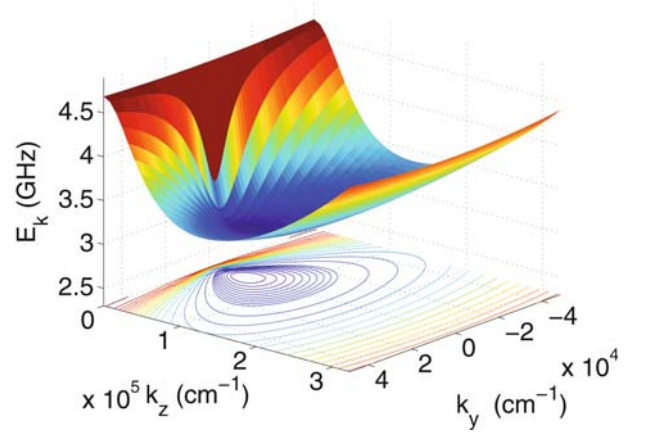


Fig. 4. (Color online) Spin-wave dispersion of the lowest mode of a YIG film with $H_e = 1000 \text{ Oe}$ and $d = 5.1 \mu\text{m}$ obtained from the numerical solution of equation (18). Starting from the minimal energy E_{min} contour lines with the spacing 20 MHz are shown to illustrate the rather flat minimum, whereas for larger energies the distance between contour lines is 100 MHz.

We parametrize the in-plane wave-vectors as

$$\mathbf{k} = |\mathbf{k}| (\cos \Theta_{\mathbf{k}} \mathbf{e}_z + \sin \Theta_{\mathbf{k}} \mathbf{e}_y), \quad (27)$$

carry out the integrations over the two infinite directions and obtain for $x_{ij} \neq 0$

$$D_{\mathbf{k}}^{xx}(x_{ij}) = D_{\mathbf{k}}(x_{ij}), \quad (28a)$$

$$D_{\mathbf{k}}^{yy}(x_{ij}) = -\sin^2 \Theta_{\mathbf{k}} D_{\mathbf{k}}(x_{ij}), \quad (28b)$$

$$D_{\mathbf{k}}^{zz}(x_{ij}) = -\cos^2 \Theta_{\mathbf{k}} D_{\mathbf{k}}(x_{ij}), \quad (28c)$$

$$D_{\mathbf{k}}^{xy}(x_{ij}) = \sin \Theta_{\mathbf{k}} D_{\mathbf{k}}(x_{ij}) \left[\frac{|\mathbf{k}|}{x_{ij}} + \frac{\text{sign}(x_{ij})}{x_{ij}^2} \right], \quad (28d)$$

where

$$D_{\mathbf{k}}(x_{ij}) = \frac{2\pi\mu^2}{a^2} |\mathbf{k}| e^{-|\mathbf{k}||x_{ij}|}. \quad (29)$$

It should be noted that in the derivation of the dipolar tensor (28a–d) we have implicitly assumed that $x_{ij} \neq 0$. This has important consequences when we also replace the sum \sum_{x_i} by the integral $a^{-1} \int_{-d/2}^{d/2} dx$. To properly account for the factor $(1 - \delta_{ij})$ in the dipole tensor in equation (7) we therefore exclude a sphere of infinitesimal radius around $x_{ij} = y_{ij} = z_{ij} = 0$ in our integrations, giving rise to the dipole matrix elements

$$D_{\mathbf{k}}^{xx} = \frac{4\pi\mu^2}{a^3} \left[\frac{1}{3} - f_{\mathbf{k}} \right], \quad (30a)$$

$$D_{\mathbf{k}}^{yy} = \frac{4\pi\mu^2}{a^3} \left[\frac{1}{3} + \sin^2 \Theta_{\mathbf{k}} (f_{\mathbf{k}} - 1) \right], \quad (30b)$$

$$D_{\mathbf{k}}^{zz} = \frac{4\pi\mu^2}{a^3} \left[\frac{1}{3} + \cos^2 \Theta_{\mathbf{k}} (f_{\mathbf{k}} - 1) \right], \quad (30c)$$

and $D_{\mathbf{k}}^{xy} = 0$. Here we have introduced the form factor [30]

$$f_{\mathbf{k}} = \frac{1 - e^{-|\mathbf{k}|d}}{|\mathbf{k}|d} = 1 - \frac{|\mathbf{k}|d}{2} + \mathcal{O}(\mathbf{k}^2 d^2), \quad (31)$$

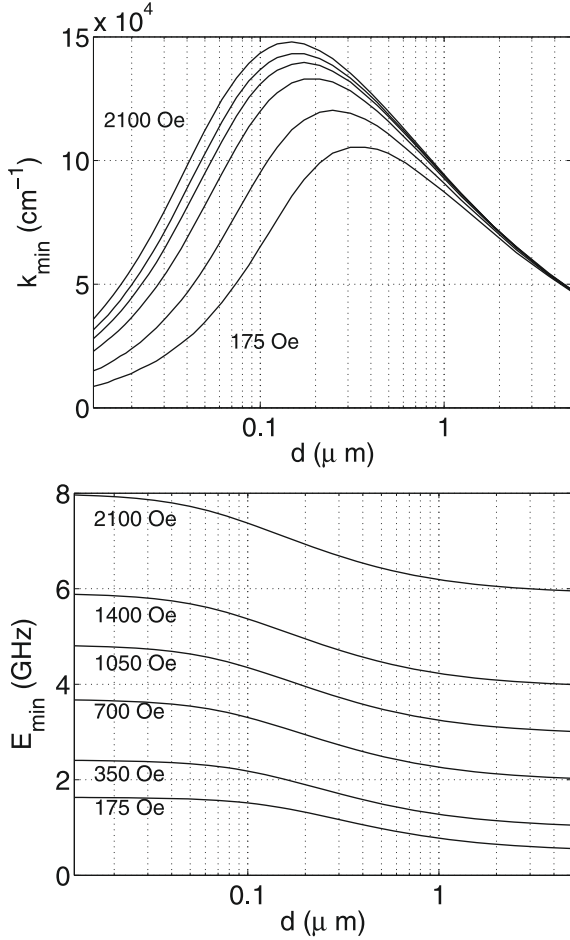


Fig. 5. Momentum k_{\min} and energy E_{\min} of the minimum in the dispersion of the lowest magnon mode for $\Theta_{\mathbf{k}} = 0$ as a function of film thickness for different magnetic fields. From top to bottom $H_e = 2100, 1400, 1050, 700, 350, 175$ Oe.

which is shown as a dashed line in Figure 6. From equations (30a–c) it is immediately obvious that our dipole elements satisfy the constraint

$$D_{\mathbf{k}}^{xx} + D_{\mathbf{k}}^{yy} + D_{\mathbf{k}}^{zz} = 0, \quad (32)$$

which follows also directly from the definition (7) of the dipolar tensor. In terms of the above dipole matrix elements we can now write the coefficients $A_{\mathbf{k}}$ and $B_{\mathbf{k}}$ as

$$A_{\mathbf{k}} = h + JS[4 - 2\cos(k_y a) - 2\cos(k_z a)] - \frac{S}{2}(D_{\mathbf{k}}^{xx} + D_{\mathbf{k}}^{yy}) + \frac{\Delta}{3}, \quad (33a)$$

$$B_{\mathbf{k}} = -\frac{S}{2}(D_{\mathbf{k}}^{xx} - D_{\mathbf{k}}^{yy}). \quad (33b)$$

The magnon dispersion $E_{\mathbf{k}}$ is now obtained by diagonalizing the effective Hamiltonian (25) via a Bogoliubov transformation [15,16], resulting in

$$E_{\mathbf{k}} = \sqrt{A_{\mathbf{k}}^2 - |B_{\mathbf{k}}|^2} = \sqrt{(A_{\mathbf{k}} - |B_{\mathbf{k}}|)(A_{\mathbf{k}} + |B_{\mathbf{k}}|)}. \quad (34)$$

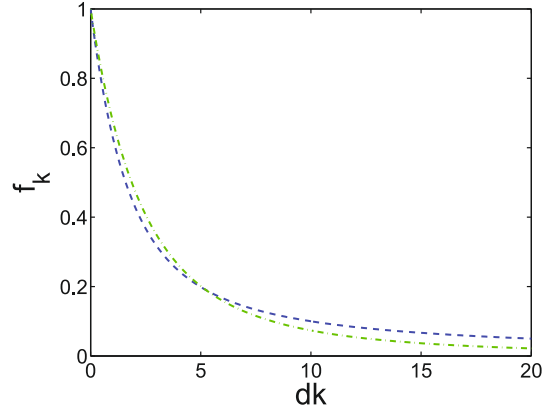


Fig. 6. (Color online) Plot of the form factors equation (31) for the uniform mode approximation (dashed) and equation (47) for the lowest eigenmode approximation (dash dotted). For the samples used in the experiments the minimum of the lowest mode is at $dk \gtrsim 5$ where the lowest eigenmode approximation is more accurate.

If we expand the terms involving the exchange interaction for small \mathbf{k} (which is sufficient for the energy range in experiments on thin films) we get

$$JS[4 - 2\cos(k_y a) - 2\cos(k_z a)] \approx JSa^2 \mathbf{k}^2 = \rho_{\text{ex}} \mathbf{k}^2. \quad (35)$$

We can then simplify the dispersion to

$$E_{\mathbf{k}} = \sqrt{[h + \rho_{\text{ex}} \mathbf{k}^2 + \Delta(1 - f_{\mathbf{k}}) \sin^2 \Theta_{\mathbf{k}}][h + \rho_{\text{ex}} \mathbf{k}^2 + \Delta f_{\mathbf{k}}]}, \quad (36)$$

which is indicated by dashed lines in Figures 2, 3 and 7. Obviously, this approximation is in good qualitative agreement with the numerical result for the lowest mode as long as $\Theta_{\mathbf{k}} \lesssim 45^\circ$. Equation (36) has been used in reference [30] to discuss the role of magnon-magnon interactions in YIG and has recently been rederived by Rezende [20]. Note, however, that in Figure 3 one clearly sees deviations from the numerical result at intermediate wave-vectors in the interval $5 \lesssim |\mathbf{k}|d \lesssim 50$. By comparing Figure 2 with Figure 3 we conclude that for the samples used in experiments [1–5,8–11] the minimum of the dispersion is exactly in this range so that better analytical approximations are needed for a more accurate description of the magnon dispersion in the vicinity of the minimum.

3.3 Lowest eigenmode approximation

To derive the dispersion of the lowest magnon mode more systematically, suppose that the $\psi_{n\mathbf{k}}(x_i)$ form (for fixed \mathbf{k}) a complete set of orthogonal functions with respect to the x -direction, i.e.,

$$\sum_{x_i} \psi_{n\mathbf{k}}^*(x_i) \psi_{m\mathbf{k}}(x_i) = \delta_{nm}, \quad (37)$$

$$\sum_n \psi_{n\mathbf{k}}(x_i) \psi_{n\mathbf{k}}^*(x_j) = \delta_{ij}. \quad (38)$$

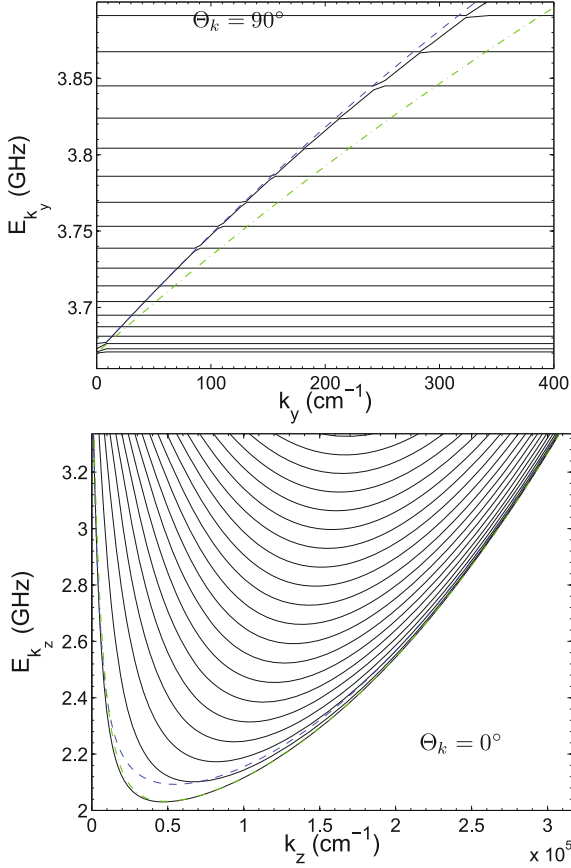


Fig. 7. (Color online) Enlarged details of Figure 3 on a linear momentum scale: spin-wave dispersion of a YIG film with thickness $d = 4040a = 5 \mu\text{m}$ for wave-vectors parallel to the external magnetic field $H_e = 700 \text{ Oe}$ ($\Theta_{\mathbf{k}} = 0^\circ$, top) and for wave-vectors perpendicular to the magnetic field ($\Theta_{\mathbf{k}} = 90^\circ$, bottom). The solid lines are exact numerical results obtained from the solution of equation (18). The dashed line is our approximate expression (36) for the lowest magnon band, using the uniform mode approximation (31) for the form factor. The dashed-dotted line is the lowest magnon band with form factor (47) given by the lowest eigenmode approximation.

We may then expand the operators $b_{\mathbf{k}}(x_i)$ in this basis,

$$b_{\mathbf{k}}(x_i) = \sum_n \psi_{n\mathbf{k}}(x_i) b_{n\mathbf{k}}, \quad (39)$$

where

$$b_{n\mathbf{k}} = \sum_{x_i} \psi_{n\mathbf{k}}^*(x_i) b_{\mathbf{k}}(x_i). \quad (40)$$

Let us retain in the expansion (39) only the $n = 0$ term,

$$b_{\mathbf{k}}(x_i) \approx \psi_{0\mathbf{k}}(x_i) b_{0\mathbf{k}}, \quad (41)$$

if we choose $\psi_{0\mathbf{k}}(x_i) = 1/\sqrt{N}$ (corresponding to the $n = 0$ term in the plane wave expansion) and identify $b_{\mathbf{k}} \equiv b_{0\mathbf{k}}$ we recover equation (24). However, a truncated expansion in plane waves seems not to be a good approximation for a system of finite width. To improve on the approxima-

tion (24) it is better to expand in terms of the eigenfunctions of the exchange matrix given in equation (17),

$$\sum_{x_j} J_{\mathbf{k}}(x_{ij}) \psi_{n\mathbf{k}}(x_j) = \lambda_{n\mathbf{k}} \psi_{n\mathbf{k}}(x_i). \quad (42)$$

For open boundary conditions these are standing waves with nodes at $x = \pm d/2$, i.e.,

$$\psi_{n\mathbf{k}}(x_i) = \sqrt{\frac{2}{N}} \sin[k_n(x_i + d/2)], \quad (43)$$

where $k_n = (n+1)\pi/d$, $n = 0, 1, \dots, N-1$. The approximation (41) then reduces to

$$b_{\mathbf{k}}(x_i) \approx \sqrt{\frac{2}{N}} \cos(k_0 x_i) b_{\mathbf{k}}, \quad (44)$$

with $k_0 = \pi/d$, and

$$b_{\mathbf{k}} = \sum_{x_i} \sqrt{\frac{2}{N}} \cos(k_0 x_i) b_{\mathbf{k}}(x_i). \quad (45)$$

Substituting equation (44) into equation (15) we obtain again an effective Hamiltonian of the form (25), but now with

$$A_{\mathbf{k}} = \frac{2}{N} \sum_{ij} \cos(k_0 x_i) \cos(k_0 x_j) A_{\mathbf{k}}(x_{ij}), \quad (46a)$$

$$B_{\mathbf{k}} = \frac{2}{N} \sum_{ij} \cos(k_0 x_i) \cos(k_0 x_j) B_{\mathbf{k}}(x_{ij}). \quad (46b)$$

Again the summations are replaced by integrations which can be carried out analytically and result in the dispersion of the form of equation (36), but with the form factor now given by

$$\begin{aligned} f_{\mathbf{k}} &= 1 - |\mathbf{k}d| \frac{|\mathbf{k}d|^3 + |\mathbf{k}d|\pi^2 + 2\pi^2(1 + e^{-|\mathbf{k}d|})}{(\mathbf{k}^2 d^2 + \pi^2)^2} \\ &= 1 - \frac{4}{\pi^2} |\mathbf{k}|d + \mathcal{O}(\mathbf{k}^2 d^2). \end{aligned} \quad (47)$$

In Figure 6 we compare this form factor with the corresponding form factor (31) obtained within the uniform mode approximation. Obviously, there are only small differences: the linear coefficient in the Taylor series is different, resulting in a smaller slope of the dispersion (36) at $\mathbf{k} = 0$. To estimate the validity of these approximations, we compare them in Figures 7 and 8 with our numerically exact results of the model (2) for experimentally relevant parameters. In Figure 7 we show the relevant details of Figure 3 on a linear momentum scale; obviously for sufficiently large wave-vectors the lowest eigenmode approximation is more accurate and practically lies on top of the numerically exact result. On the other hand, for small wave-vectors the uniform mode approximation fits better, as illustrated by the lower part of Figure 7. A more quantitative comparison between these two approximations for wave-vectors parallel to the magnetic field and different

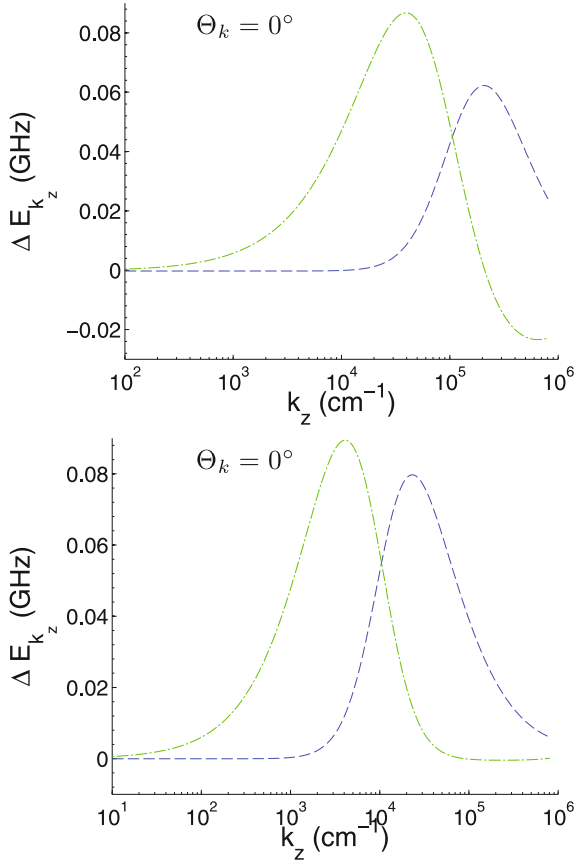


Fig. 8. (Color online) Accuracy of our two analytical approximations for the lowest magnon mode for a YIG film with $N = 400$ layers (top) and $N = 4040$ layers (bottom). Dashed line: difference between the numerical result and the uniform mode approximation; dash-dotted line: difference between the numerical result and the lowest eigenmode approximation.

film thickness is shown in Figure 8. Roughly, for $d|\mathbf{k}| \lesssim 5$ the uniform mode approximation fits better, while for $d|\mathbf{k}| \gtrsim 5$ the lowest eigenmode approximation gives a better agreement with the numerical results. As there are not many states at small wave-vectors, we believe that the lowest eigenmode approximation is more suitable for a quantitative description of the magnon dispersion, in particular if one is interested in physical effects related to the dispersion minimum at \mathbf{k}_{\min} . On the other hand, both analytical approximations describe the quasi-continuous surface mode for large $\Theta_{\mathbf{k}} > 45^\circ$ rather accurately as long as the wave-vectors are sufficiently small so that the dispersion curves tend upwards due to the presence of exchange interaction [7] and hybridize.

4 Conclusions and outlook

In this work we have presented a comprehensive discussion of the spin-wave spectra of experimentally relevant samples of thin films of the magnetic insulator YIG. Starting from an effective spin- S Heisenberg Hamiltonian with exchange and dipole-dipole interactions on a cubic lattice,

we have used a truncated Holstein-Primakoff transformation to obtain an effective quadratic boson Hamiltonian whose eigen-energies can be identified with the magnon energies. We have then used numerical methods to calculate the magnon dispersions for experimentally relevant films with thickness corresponding to a few thousand lattice spacings without further approximations. In order to carry out the dipolar sums entering the secular determinant, the use of efficient Ewald summation techniques was necessary. We have also estimated the accuracy of two different analytical approximations for the lowest magnon band: the uniform mode approximation (where the transverse spatial variation of the eigenmodes is ignored) and the lowest eigenmode approximation (where the lowest transverse mode is approximated by the lowest eigenmode of the exchange matrix). For realistic films, the latter approximation is more accurate for wave-vectors in the vicinity of the dispersion minimum.

In contrast to the phenomenological approach based on the Landau-Lifshitz equation [6,7], in our microscopic approach it is straightforward to systematically take into account interaction effects. In future work we shall carefully derive the momentum-dependent interaction vertices of the bosonized effective in-plane Hamiltonian using the lowest eigenmode approximation, which according to our investigations in Section 3 is more accurate in the experimentally interesting regime of wave-vectors close to \mathbf{k}_{\min} . Although rough estimates of the interactions vertices can be found in the literature [30], more accurate microscopic calculations which properly take into account the momentum-dependence of the vertices are needed in order to gain a better understanding of the role of spin-wave interactions in the experiments [1–5,8–11]. For example, it would be interesting to know the intrinsic damping of the lowest magnon mode for wave-vectors close to \mathbf{k}_{\min} due to magnon-magnon interactions.

We would like to thank A.A. Serga, T. Neumann and P. Prioznia for helpful discussions and gratefully acknowledge financial support by the SFB/TRR49 and the DAAD/PROBRAL-program.

Appendix: Dipolar sums

For the calculation of the slowly converging sums in equation (20) we introduce the quantity

$$I_{\mathbf{k}}(x_{ij}) = \mu^2 \sum_{y_{ij}, z_{ij}} \frac{e^{-i(k_y y_{ij} + k_z z_{ij})}}{(x_{ij}^2 + y_{ij}^2 + z_{ij}^2)^{5/2}}, \quad (\text{A.1})$$

and get the dipolar sums as derivatives,

$$D_{\mathbf{k}}^{yy}(x_{ij}) = \left[\frac{\partial^2}{\partial k_z^2} - 2 \frac{\partial^2}{\partial k_y^2} - x_{ij}^2 \right] I_{\mathbf{k}}(x_{ij}), \quad (\text{A.2a})$$

$$D_{\mathbf{k}}^{zz}(x_{ij}) = \left[\frac{\partial^2}{\partial k_y^2} - 2 \frac{\partial^2}{\partial k_z^2} - x_{ij}^2 \right] I_{\mathbf{k}}(x_{ij}), \quad (\text{A.2b})$$

$$D_{\mathbf{k}}^{xx}(x_{ij}) = \left[\frac{\partial^2}{\partial k_y^2} + \frac{\partial^2}{\partial k_z^2} + 2x_{ij}^2 \right] I_{\mathbf{k}}(x_{ij}), \quad (\text{A.2c})$$

$$D_{\mathbf{k}}^{xy}(x_{ij}) = i 3x_{ij} \frac{\partial}{\partial k_y} I_{\mathbf{k}}(x_{ij}). \quad (\text{A.2d})$$

Note the symmetry $D_{\mathbf{k}}^{xx} = D_{\tilde{\mathbf{k}}}^{xx}$ and the relation $D_{\mathbf{k}}^{yy} = D_{\tilde{\mathbf{k}}}^{zz}$ with $\tilde{\mathbf{k}} = k_z \mathbf{e}_y + k_y \mathbf{e}_z$. To evaluate the above expressions, we consider the cases $x_{ij} \neq 0$ and $x_{ij} = 0$ separately.

A.1 Case $\mathbf{x}_{ij} \neq \mathbf{0}$

Using the identity

$$\int_0^\infty x^{n-1/2} e^{-\alpha x} dx = \sqrt{\pi} 2^{-n} \alpha^{-n-1/2} (2n-1)!!, \quad (\text{A.3})$$

where $n > 0$, $\text{Re } \alpha > 0$, and introducing the dummy variable ε to check the results, we can rewrite

$$I_{\mathbf{k}}(x_{ij}) = \mu^2 \frac{4}{3} \sqrt{\frac{\varepsilon^5}{\pi}} \int_0^\infty dt t^{3/2} e^{-x_{ij}^2 \varepsilon t} \times \sum_{y_{ij} z_{ij}} e^{-(y_{ij}^2 + z_{ij}^2) \varepsilon t} e^{-i(k_y y_{ij} + k_z z_{ij})}. \quad (\text{A.4})$$

We split the integral in two parts and use Ewald's method [24,31]

$$\sum_{\mathbf{r}} e^{-\varepsilon t |\mathbf{r}|^2} e^{-i\mathbf{k} \cdot \mathbf{r}} = \frac{\pi}{a^2 \varepsilon t} \sum_{\mathbf{g}} e^{-\frac{|\mathbf{k} + \mathbf{g}|^2}{4\varepsilon t}}, \quad (\text{A.5})$$

to transform the lattice sum into a lattice sum in reciprocal space, where $\mathbf{g} = g_y \mathbf{e}_y + g_z \mathbf{e}_z$ is a reciprocal lattice vector. This yields

$$I_{\mathbf{k}}(x_{ij}) = \frac{4}{3} \mu^2 \left[\frac{\sqrt{\pi \varepsilon^3}}{a^2} \sum_{\mathbf{g}} \int_0^1 dt t^{1/2} e^{-\frac{|\mathbf{k} + \mathbf{g}|^2}{4\varepsilon t} - x_{ij}^2 \varepsilon t} + \sqrt{\frac{\varepsilon^5}{\pi}} \sum_{\mathbf{r}} e^{-i\mathbf{k} \cdot \mathbf{r}} \varphi_{3/2}(|\mathbf{r}_{ij}|^2 \varepsilon) \right], \quad (\text{A.6})$$

where

$$\varphi_\nu(z) = \int_1^\infty dt t^\nu e^{-zt} \quad (\text{A.7})$$

is the Misra function,¹ which for $\nu = 3/2$ and $z \equiv x > 0$ can also be written as

$$\varphi_{3/2}(x) = e^{-x} \frac{3+2x}{2x^2} + \frac{3\sqrt{\pi} \text{Erfc}(\sqrt{x})}{4x^{5/2}}. \quad (\text{A.8})$$

Evaluating the integral in equation (A.6) for $p > 0$ and $q^2 > 0$ using

$$\int_0^1 dt t^{1/2} e^{-q^2 t} e^{-p^2/t} = -\frac{e^{-p^2-q^2}}{q^2} + \frac{\sqrt{\pi}}{4q^3} \left[e^{-2pq} (1+2pq) \text{Erfc}(p-q) + e^{2pq} (-1+2pq) \text{Erfc}(p+q) \right], \quad (\text{A.9})$$

¹ The Misra function is defined in terms of the exponential integral $\text{Ei}_\nu(z) = \int_1^\infty dx e^{-xz} x^{-\nu}$ via $\varphi_\nu(z) = \text{Ei}_{-\nu}(z)$.

we can calculate the derivatives according to equations (A.2) and finally get the result for the sums of the dipole interactions between spins located in different atomic layers,

$$D_{\mathbf{k}}^{xx}(x_{ij}) = -\frac{\pi \mu^2}{a^2} \sum_{\mathbf{g}} \left\{ \frac{8\sqrt{\varepsilon}}{3\sqrt{\pi}} e^{-p^2-q^2} - |\mathbf{k} + \mathbf{g}| f(p, q) \right\} - \frac{4\varepsilon^{5/2} \mu^2}{3\sqrt{\pi}} \sum_{\mathbf{r}} (\mathbf{r}_{ij}^2 - 3x_{ij}^2) \cos(k_y y_{ij}) \cos(k_z z_{ij}) \varphi_{3/2}(\mathbf{r}_{ij}^2 \varepsilon), \quad (\text{A.10a})$$

$$D_{\mathbf{k}}^{yy}(x_{ij}) = \frac{\pi \mu^2}{a^2} \sum_{\mathbf{g}} \left\{ \frac{4\sqrt{\varepsilon}}{3\sqrt{\pi}} e^{-p^2-q^2} - \frac{(k_y + g_y)^2}{|\mathbf{k} + \mathbf{g}|} f(p, q) \right\} - \frac{4\varepsilon^{5/2} \mu^2}{3\sqrt{\pi}} \sum_{\mathbf{r}} (\mathbf{r}_{ij}^2 - 3y_{ij}^2) \cos(k_y y_{ij}) \cos(k_z z_{ij}) \varphi_{3/2}(\mathbf{r}_{ij}^2 \varepsilon), \quad (\text{A.10b})$$

$$D_{\mathbf{k}}^{xy}(x_{ij}) = i \frac{\pi \mu^2}{a^2} \text{sig}(x_{ij}) \sum_{\mathbf{g}} (k_y + g_y) f(p, q) + i \frac{4\varepsilon^{5/2} \mu^2}{\sqrt{\pi}} x_{ij} \sum_{\mathbf{r}} y_{ij} \sin(k_y y_{ij}) \cos(k_z z_{ij}) \varphi_{3/2}(\mathbf{r}_{ij}^2 \varepsilon), \quad (\text{A.10c})$$

where we have used the abbreviations $q = x_{ij} \sqrt{\varepsilon}$ and $p = |\mathbf{k} + \mathbf{g}| / (2\sqrt{\varepsilon})$ and have introduced the function

$$f(p, q) = e^{-2pq} \text{Erfc}(p-q) + e^{2pq} \text{Erfc}(p+q). \quad (\text{A.11})$$

For the simple cubic lattice the components of the reciprocal lattice vectors are $g_y = 2\pi m$, $g_z = 2\pi n$, $\{m, n\} \in \mathbb{Z}$. Note that this result is independent of the variable ε which shifts the weight from the sums in real space to the sums in reciprocal space as $\varepsilon \rightarrow 0$ and therefore simplifies to the sums given in reference [22] for $\varepsilon = 0$.

A.2 Case $\mathbf{x}_{ij} = \mathbf{0}$

In this case we have to exclude the point $\mathbf{r} = \mathbf{0}$ because there is no self interaction. We therefore introduce the dummy variable $\mathbf{x} = y \mathbf{e}_y + z \mathbf{e}_z$,

$$I_{\mathbf{k}}(x_{ij} \equiv 0) = I_{\mathbf{k}} = \sum_{\mathbf{r}} \frac{e^{-i\mathbf{k} \cdot \mathbf{r}}}{|\mathbf{r} - \mathbf{x}|^5}. \quad (\text{A.12})$$

Using equation (A.3) we can rewrite equation (A.12) and use the transformation on the reciprocal lattice

$$\sum_{\mathbf{r}} e^{-i\mathbf{k} \cdot \mathbf{r} - |\mathbf{x} - \mathbf{r}|^2 \varepsilon t} = \frac{\pi}{a^2 \varepsilon t} \sum_{\mathbf{g}} e^{i(\mathbf{g} + \mathbf{k}) \cdot \mathbf{x} - \frac{|\mathbf{g} + \mathbf{k}|^2}{4\varepsilon t}}. \quad (\text{A.13})$$

We subtract $1/|\mathbf{x}|^5$ from the sum on the left, which is equivalent to removing this first term in the sum over \mathbf{r} in our dipole sum. In the limit $\mathbf{x} \rightarrow 0$ we obtain,

$$I_{\mathbf{k}} = \frac{8\varepsilon^{3/2}\sqrt{\pi}}{9a^2} \sum_{\mathbf{g}} \left[e^{-p^2} (1 - p^2) + 2\sqrt{\pi} p^3 \text{Erfc}(p) \right] + \frac{8\varepsilon^{5/2}}{9\sqrt{\pi}} \sum_{\mathbf{r}}' \left[e^{-\mathbf{r}^2\varepsilon} (1 - 2\mathbf{r}^2\varepsilon) + 2\sqrt{\pi} |\mathbf{r}| \sqrt{\varepsilon} \text{Erfc}(|\mathbf{r}| \sqrt{\varepsilon}) \right] - \frac{8\varepsilon^{5/2}}{15\pi}. \quad (\text{A.14})$$

After taking the derivatives according equation (A.2) we note that we get for the dipolar sums the limit $q = x_{ji}\varepsilon \rightarrow 0$ of equation (A.10) and therefore the removing of the origin does not make any difference in the calculation of the dipole sums except for omitting the term $\mathbf{r} = 0$ in the real space sums.

References

1. S.O. Demokritov, V.E. Demidov, O. Dzyapko, G.A. Melkov, A.A. Serga, B. Hillebrands, A.N. Slavin, *Nature* **443**, 430 (2006)
2. V.E. Demidov, O. Dzyapko, S.O. Demokritov, G.A. Melkov, A.N. Slavin, *Phys. Rev. Lett.* **99**, 037205 (2007)
3. O. Dzyapko, V.E. Demidov, S.O. Demokritov, G.A. Melkov, A.N. Slavin, *New J. Phys.* **9**, 64 (2007)
4. V.E. Demidov, O. Dzyapko, S.O. Demokritov, G.A. Melkov, A.N. Slavin, *Phys. Rev. Lett.* **100**, 047205 (2008)
5. S.O. Demokritov, V.E. Demidov, O. Dzyapko, G.A. Melkov, A.N. Slavin, *New J. Phys.* **10**, 045029 (2008)
6. B.A. Kalinikos, A.N. Slavin, *J. Phys. C: Solid State Phys.* **19**, 7013 (1986)
7. *Linear and Nonlinear Spin Waves in Magnetic Films and Superlattices*, edited by M.G. Cottam (World Scientific, Singapore, 1994)
8. A.A. Serga, A.V. Chumak, A. Andre, G.A. Melkov, A.N. Slavin, S.O. Demokritov, B. Hillebrands, *Phys. Rev. Lett.* **99**, 227202 (2007)
9. S. Schäfer, A.V. Chumak, A.A. Serga, G.A. Melkov, B. Hillebrands, *Appl. Phys. Lett.* **92**, 162514 (2008)
10. A.V. Chumak, A.A. Serga, B. Hillebrands, G.A. Melkov, V. Tiberkevich, A.N. Slavin, *Phys. Rev. B* **79**, 014405 (2009)
11. T. Neumann, A.A. Serga, B. Hillebrands, *Appl. Phys. Lett.* **93**, 252501 (2008)
12. T. Holstein, H. Primakoff, *Phys. Rev.* **58**, 1098 (1940)
13. F.J. Dyson, *Phys. Rev.* **102**, 1217, 1230 (1956)
14. S. Maleev, *Zh. Eksper. Teor. Fiz.* **33**, 1010 (1957)
15. A.I. Akhiezer, V.G. Bar'yakhtar, S.V. Peletminskii, *Spin Waves* (North Holland, Amsterdam, 1968)
16. D.C. Mattis, *The theory of magnetism made simple* (World Scientific, Singapore, 2006)
17. R.P. Erickson, D.L. Mills, *Phys. Rev. B* **43**, 10715 (1991)
18. R.P. Erickson, D.L. Mills, *Phys. Rev. B* **44**, 11825 (1991)
19. J.J.M. Pereira, M.G. Cottam, *J. Appl. Phys.* **85**, 4949 (1999)
20. S.M. Rezende, *Phys. Rev. B* **79**, 060410 (2009)
21. R.N. Costa Filho, M.G. Cottam, G.A. Farias, *Solid State Commun.* **108**, 439 (1998)
22. R.N. Costa Filho, M.G. Cottam, G.A. Farias, *Phys. Rev. B* **62**, 6545 (2000)
23. H. Benson, D.L. Mills, *Phys. Rev.* **178**, 839 (1969)
24. J.M. Ziman, *Principles of the Theory of Solids* (Cambridge University Press, Cambridge, 1979)
25. M.P. Kostylev, G. Gubbiotti, J.G. Hu, G. Carlotti, T. Ono, R.L. Stamps, *Phys. Rev. B* **76**, 054422 (2007)
26. V. Cherepanov, I. Kolokolov, V. L'vov, *Phys. Rep.* **229**, 81 (1993)
27. M.A. Gilleo, S. Geller, *Phys. Rev.* **110**, 73 (1958)
28. B.R. Tittmann, *Solid State Commun.* **13**, 463 (1973)
29. A.G. Gurevich, G.A. Melkov, *Magnetization Oscillations and Waves* (CRC Press, Boca Raton, 1996)
30. I.S. Tupitsyn, P.C.E. Stamp, A.L. Burin, *Phys. Rev. Lett.* **100**, 257202 (2008)
31. L. Bartosch, L. Balents, S. Sachdev, *Ann. Phys. (New York)* **321**, 1528 (2006)